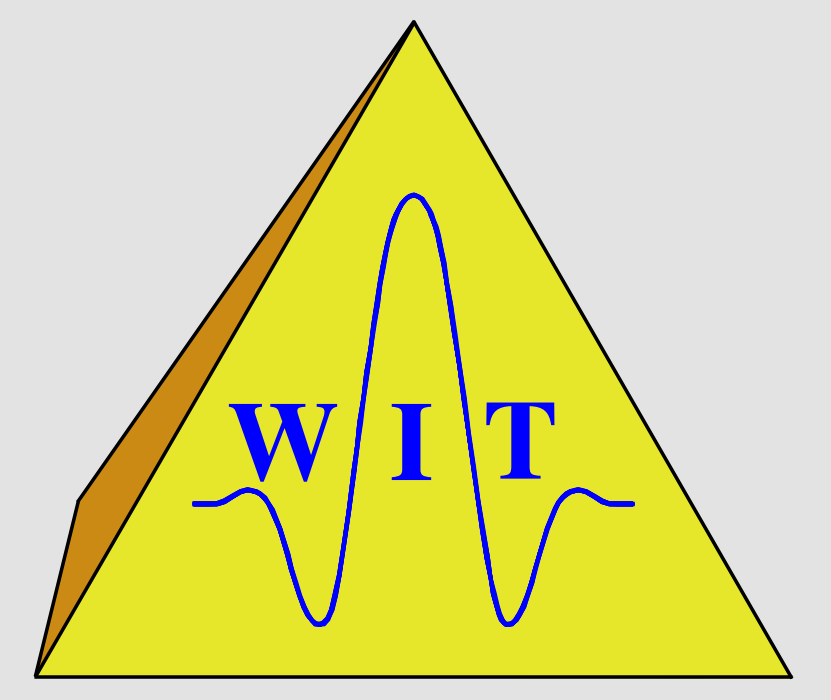


2D CO CRS stack for multi-component seismic reflection data

Tim Boelsen and Jürgen Mann

Geophysical Institute, University of Karlsruhe, Germany



Summary

The Common-Reflection-Surface stack as an alternative to conventional stacking methods has so far mainly been applied to single-component data. We introduce an approach that allows to generate separate stacks of compressional and shear waves from multi-component seismic reflection data. Based on the traveltimes approximation for finite offset, the polarization is analyzed during the search for the optimum orientation and curvature of the Common-Reflection-Surface stacking operator. We apply this approach to a simple synthetic data set and obtain stacked sections and kinematic wavefield attribute sections separately for PP and PS reflection events.

Introduction

Several well-known stacking tools were established to simulate zero-offset (ZO) sections from multi-coverage, seismic reflection prestack data, e.g., the common-midpoint (CMP) stack and the normal-moveout (NMO)/dip-moveout (DMO)/stack sequence. However, these methods do not make full use of the available reflection energy during stacking and deliver less information for further imaging steps compared to novel approaches.

One of the novel approaches is the Common-Reflection-Surface (CRS) stack (e.g., Mann et al., 1999; Jäger et al., 2001). Compared to conventional stacking methods the CRS stack has the following advantages:

- Similarly as in high-density stacking velocity analysis, the optimum CRS stacking operator is determined fully automated by means of coherence analysis. Thus, it is an entirely *data-driven* method.
- For each sample of the section to be simulated, the operator utilizes the full multi-coverage data volume within a spatial aperture during the imaging process. The operator defines an entire *stacking surface* with a spatial extension also in midpoint direction. Thus, much more traces contribute to the CRS stack result yielding *higher signal-to-noise (S/N) ratios*.
- The parameterization of the CRS stacking operator is based on an isotropic, inhomogeneous model with curved reflectors. Therefore, the operator fits the actual reflection events in the prestack data often better than conventional methods based on simpler assumptions.
- As a by-product of the CRS stack, *kinematic wavefield attribute and coherence sections* are obtained which can be used for further applications like different kinds of inversion schemes (see, e.g., Duvenceck, 2004; Müller, 2005).

Originally developed to stack single-component prestack data into a ZO section, the CRS method was extended to stack prestack data into a selected finite-offset (FO) gather (Zhang et al., 2001), e.g., into a common-offset (CO) gather. Bergler (2001) showed that this so-called 2D CO CRS stacking operator can also be used to describe traveltimes of S-waves as well as PS converted waves.

Here, we introduce a new approach to distinguish between PP- and PS-waves during the CRS stack to obtain stacked sections, kinematic wavefield attribute sections, and coherence sections for each wave type.

2D CO CRS stacking operator

This operator approximates the traveltimes of a reflection event in the vicinity of an arbitrarily selected point P_0 (t_0, m_0, h_0) on the reflection event. For any other trace located at (m, h) in the vicinity of (m_0, h_0) , the hyperbolic traveltimes approximation derived from paraxial ray theory (Bergler, 2001; Zhang et al., 2001) reads

$$t^2(\Delta m, \Delta h) = \left[t_0 + \left(\frac{\sin \beta_G}{v_G} - \frac{\sin \beta_S}{v_S} \right) \Delta m + \left(\frac{\sin \beta_G}{v_G} + \frac{\sin \beta_S}{v_S} \right) \Delta h \right]^2 + t_0 \left[2\Delta h \Delta m \left(\frac{K_3 \cos^2 \beta_G}{v_G} + \frac{K_2 \cos^2 \beta_S}{v_S} \right) + \Delta m^2 \left(\frac{4K_1 - 3K_3}{v_G} \frac{\cos^2 \beta_G}{v_G} - \frac{K_2 \cos^2 \beta_S}{v_S} \right) + \Delta h^2 \left(\frac{K_3 \cos^2 \beta_G}{v_G} - \frac{K_2 \cos^2 \beta_S}{v_S} \right) \right]. \quad (1)$$

In Equation (1), t_0 denotes the traveltimes along the central ray, m_0 the midpoint between source and receiver associated with this ray, h_0 is their half-offset. The midpoint and offset displacements of the considered central and paraxial rays are defined as $\Delta h = h - h_0$ and $\Delta m = m - m_0$. The near-surface velocities of the considered wave type are denoted by v_S and v_G at source and receiver, respectively. The remaining five parameters, the kinematic wavefield attributes, are related to propagation directions and curvatures of wavefronts (Bergler, 2001):

- β_S and β_G are the incidence/emergence angles of the central ray at source and receiver,
- the wavefront curvature K_1 is observed at the receiver due to a common-shot (CS) experiment,
- K_2 and K_3 are curvatures of wavefronts related to a hypothetical CMP experiment measured at source and receiver, respectively.

Although originally derived for surface seismic geometries, this traveltimes approximation also holds for OBS geometries with virtually horizontal seafloor (Boelsen and Mann, 2005).

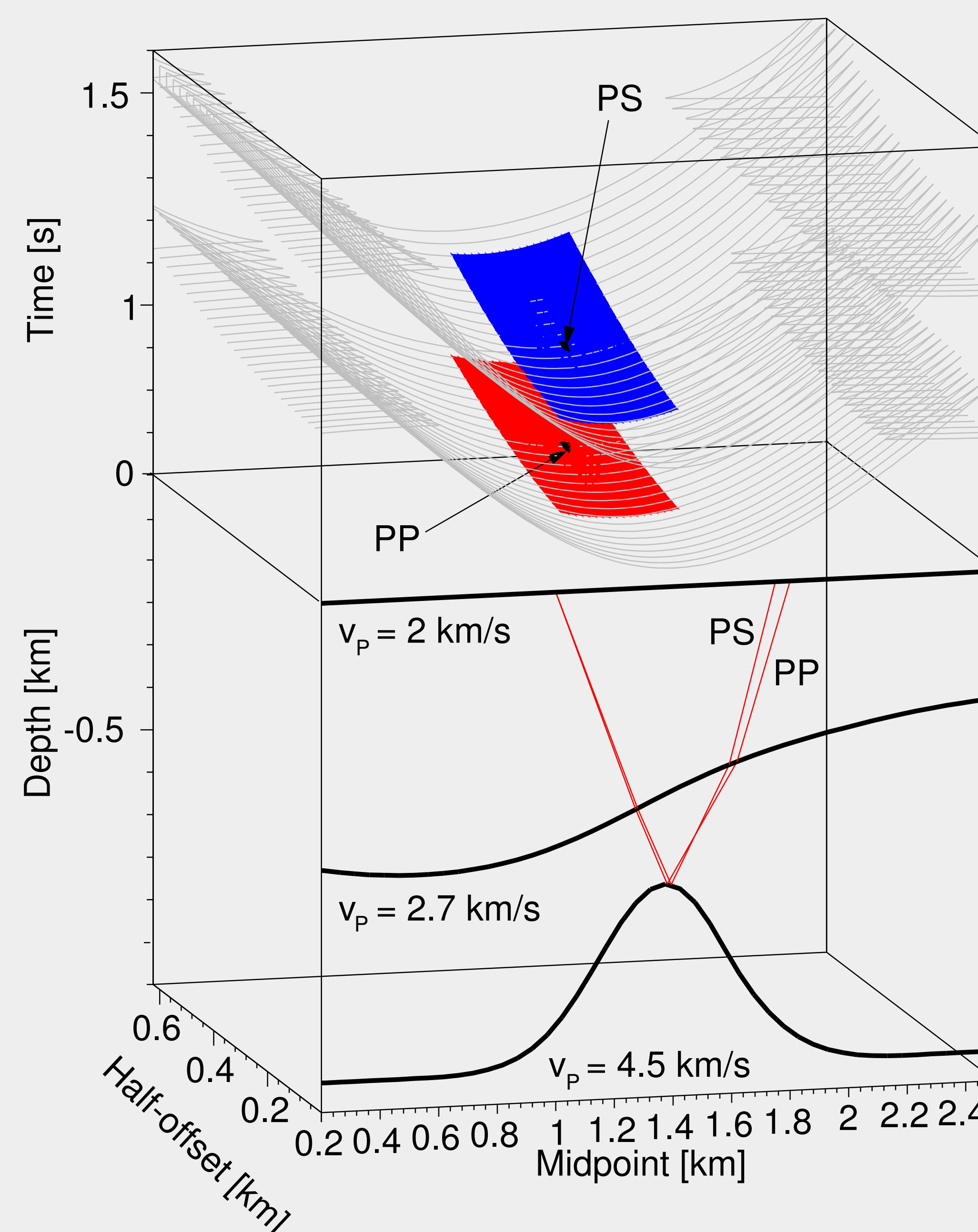


Figure 1: Lower part: a simple 2D model with homogeneous layers. Upper part: forward-calculated traveltimes of PP- and PS-waves reflected at the second interface (gray CO traveltimes curves). The CO CRS stacking surfaces for PP- and PS-waves associated with the two depicted central rays are visualized in red and blue, respectively. The near-surface velocity v_G at the receivers in Equation (1) has to be chosen according to the respective wave type.

Including polarization information

Assuming an isotropic layer below the receiver line, the polarization directions of P- and S-waves emerging at the receivers are directly related to the propagation directions of the emerging (hypothetical) wavefronts. For the receiver associated with the central ray, this direction is given by the wavefield attribute β_G , for all other receivers it has to be extrapolated from the (known) attributes associated with the central ray.

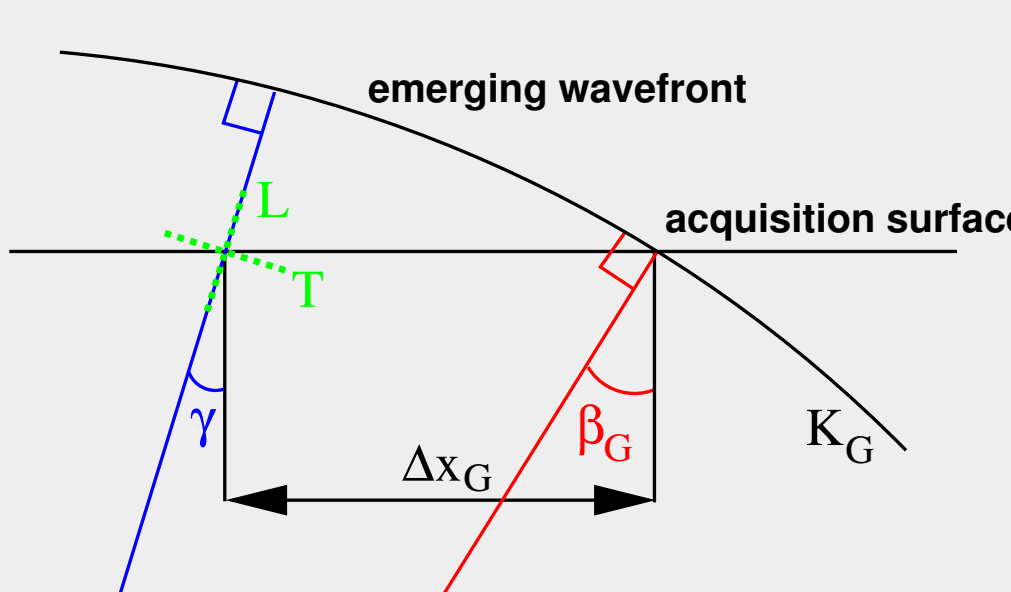


Figure 2: Definition of emergence angles for central (red) and paraxial (blue) ray. The expected transversal (T) and longitudinal (L) polarization directions are indicated in green. See main text for K_G and Δx_G .

In the second-order approximation inherent to the CRS stack approach, we can assume the radius of curvature $R_G = 1/K_G$ of the emerging wavefront at the receiver to be constant within the stacking aperture. Also assuming the near-surface velocity at the receiver to be constant, the emergence angle γ of a paraxial ray can be extrapolated by (modified after Höcht et al., 1999)

$$\sin \gamma = \text{signum}(R_G) \frac{R_G \sin \beta_G + \Delta x_G}{\sqrt{R_G^2 + 2R_G \Delta x_G \sin \beta_G + \Delta x_G^2}}, \quad (2)$$

where Δx_G is the horizontal receiver displacement associated with the central and paraxial ray. Note that K_G depends on the considered source/receiver configuration. It is given by a linear combination of the two curvatures K_1 and K_3 defined at the receiver (Bergler, 2001):

$$K_G = K_1 \left(1 + \frac{1}{l} \right) - \frac{K_3}{l}, \quad (3)$$

where l is a real number describing the arbitrary measurement configuration $\Delta x_G = l \Delta x_S$. Equation (2) does not consider the free surface or the effect of the seafloor in OBS data. Appropriate corrections are required when applying the approach to real data.

We assume the data to be acquired with two components, namely with global vertical (V) and horizontal (H) components in the plane defined by the source/receiver line, see Figure 3. Two different types of waves are considered, PP- and PS-waves. The general idea is to automatically transform the multi-component data into longitudinal and transversal components:

- During the CO CRS stack, $\sin \beta_G / v_G$ is determined. Depending on the chosen near-surface velocity, P- or S-wave velocity, we calculate the emergence angles β_G for emerging P- or S-waves propagating along the respective central ray.
- After the extrapolation of the emergence angles γ according to Equation (2) we rotate the global coordinate system defined by the vertical and horizontal components V and H by γ :

$$\begin{pmatrix} T \\ L \end{pmatrix} = \begin{pmatrix} \cos \gamma & \sin \gamma \\ -\sin \gamma & \cos \gamma \end{pmatrix} \begin{pmatrix} H \\ V \end{pmatrix}, \quad (4)$$

where L and T denote the longitudinal and transversal components, respectively. The situation after the rotation is also depicted in Figure 3.

To actually distinguish between both wave types we make use of the above made assumption of isotropy below the receiver:

- Choosing in a first step the near-surface velocity v_G to be the P-wave velocity, the direction of the ray at the receiver given by β_G^P defines the polarization direction of an emerging P-wave propagating along this ray. Thus, the amplitude of this PP-reflection is given by the longitudinal component L.
- In a second step, the S-wave velocity is used as the near-surface velocity at the receiver. In that case the expected polarization direction of an emerging S-wave propagating along that ray would then be normal to the ray direction, defined by β_G^S , and the amplitude of this PS-reflection is given by the transversal component T.

All coherence analyses and stacking operations are performed in these coordinate systems which, of course, depend on the currently investigated attribute set. Thus, operator orientation and shape are combined with polarization information on the fly.

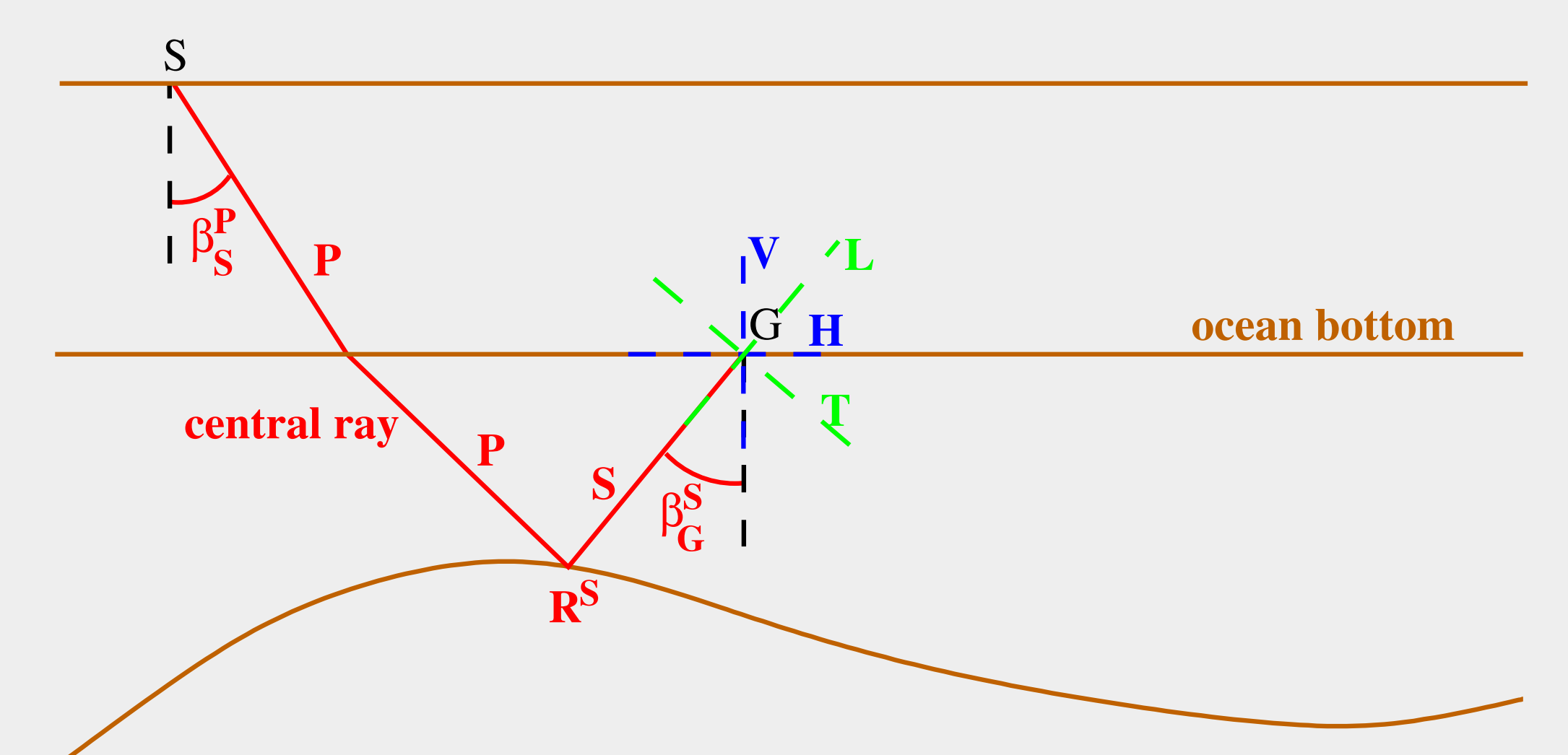
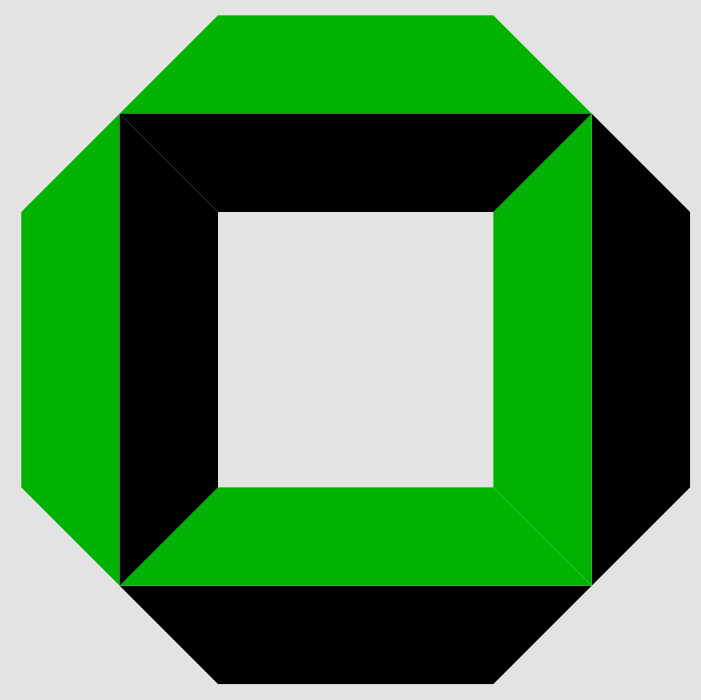


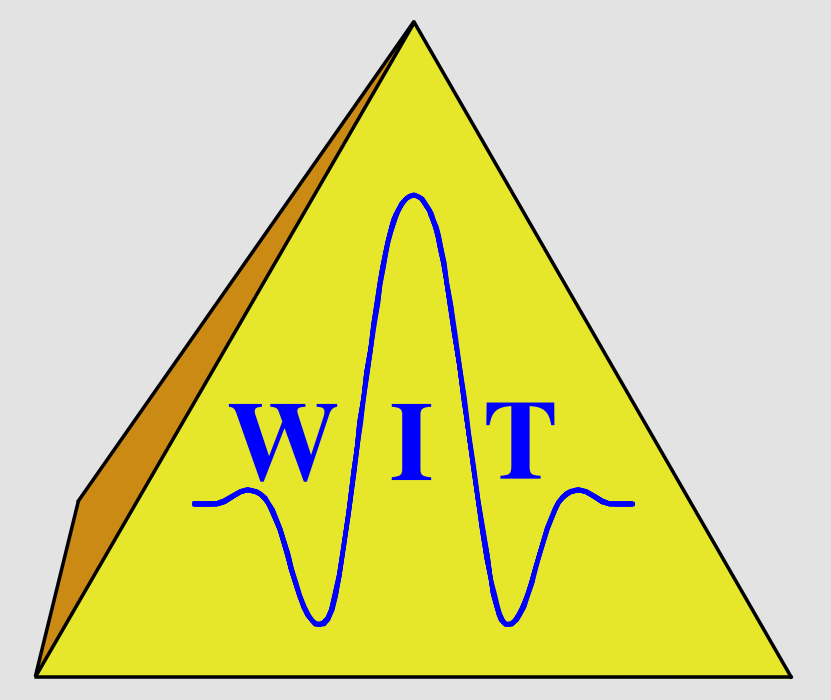
Figure 3: After the rotation of the vertical (V) and horizontal (H) components we obtain the longitudinal (L) and transversal (T) components. For the depicted case of a central PS-ray, γ coincides with β_G . Note that this strategy is not restricted to the OBS geometry illustrated here.



2D CO CRS stack for multi-component seismic reflection data

Tim Boelsen and Jürgen Mann

Geophysical Institute, University of Karlsruhe, Germany



Implementation strategy

For a given set of the five wavefield attributes, R_G and γ can always be calculated. The singularity of Equation (2) for the common-receiver gather, $R_G = \Delta x_G = 0$, is removable (Boelsen, 2005). β_G and γ allow to extract the longitudinal and transversal components from the multi-component data for the coherence analysis as well as the stack.

A simultaneous search for all five parameters is quite time consuming. Therefore, the global optimization problem is often decomposed into several (global) optimization steps performed with subsets of the entire prestack data such that the maximum number of simultaneously searched-for parameters is reduced to two. For the CO CRS stack, Bergler (2001) implemented such a search strategy which starts with a two-parameter search in the CMP gather. However, the need to determine R_G and γ during the stack requires a different search strategy:

- Search for β_G and K_1 in the CS gather. In this case, $K_G = K_1$ such that γ is always well defined. This yields separate CS-stacked CO sections for PP- and PS-waves.
- Two successive one-parameter searches (or alternatively one two-parameter search) in the simulated CO sections. This yields the second angle β_S and a combination of K_1 , K_2 , and K_3 . Polarization does not have to be considered, as the PP- and PS-events are already separated in the simulated CO sections.
- A final one-parameter search in the CMP gather for a combination of K_2 and K_3 . This search is performed in the multi-component data. Thus, polarization has to be considered with $K_G = K_3$.
- Stack along the full spatial operator in the full prestack data set. For each contributing trace, K_G is given by Equation (3). This yields the final CRS stacked CO sections for PP- and PS-reflections. Additionally, the five wavefield attribute sections can be computed for both wave types.

A first data example

To evaluate our approach, the proposed strategy was applied to a very simple synthetic 2D land data set. The model consists of two homogeneous layers separated by a single horizontal interface at a depth of 2 km. The P-wave velocity v_P above the reflector is 2 km/s, the S-wave velocity v_S is $v_P/\sqrt{3}$.

For this model, a two-component multi-coverage prestack data set was generated which contains the primary PP- and PS-reflections. Shot spacing was 25 m, receiver spacing 50 m. As seismic signal, a zero-phase Ricker wavelet of 30 Hz peak frequency was used. The sampling interval was 4 ms. Free-surface effects were not modeled as they are not yet considered in our approach.

Random noise was added to the data set such that all CO prestack sections look with respect to their S/N ratio similar to the ones for half-offset $h = -0.5$ km, see Figure 4 which shows a) the vertical and b) the horizontal component. Of course, both reflection events are present on both components. It is the aim of this data example to distinguish between the PP- and the PS-reflections during the CO CRS stacking procedure in order to generate separate stacked sections as well as wavefield attribute sections for both events for half-offset $h = -0.5$ km.

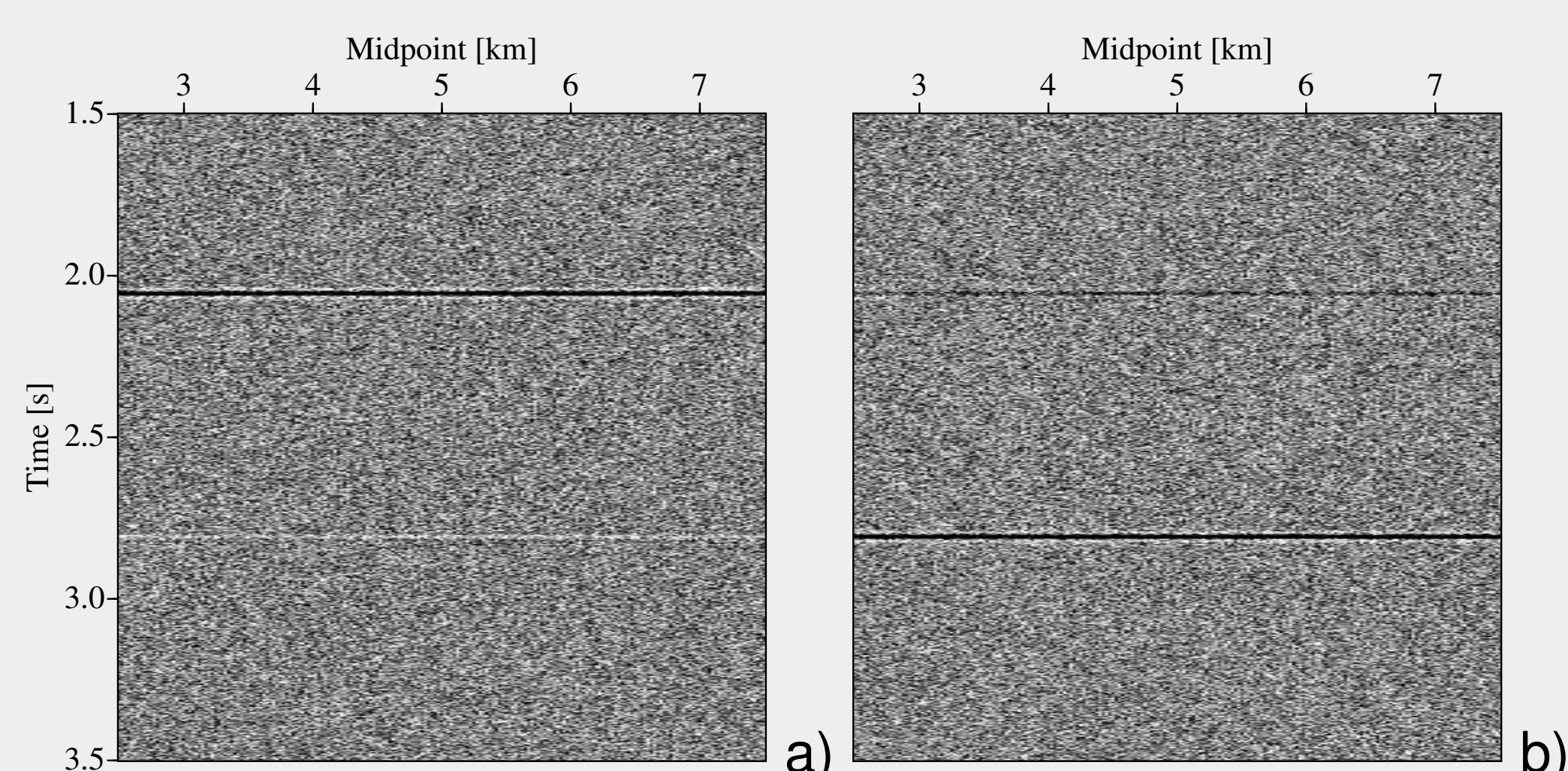


Figure 4: CO sections for half-offset $h = -0.5$ km extracted from the synthetic prestack data: a) vertical and b) horizontal component. Both events can be observed on both components, the upper event is the PP-reflection, the lower the PS-reflection.

We abstain from presenting all the intermediate results from the CS, CO, and CMP search and stack. Instead, only the final CO CRS stack results are shown.

The upper part of Figure 5 depicts the CO sections simulated with the CO CRS stack for a) PP- and b) PS-reflections. The stacked sections show a dramatically increased S/N ratio compared with the prestack data (Figure 4) and the intermediate stack results (not shown) which is caused by the spatial stacking operator. Thus, much more traces contribute to each sample of the CO CRS stack sections. The successful distinction between both wave types is clearly visible in the stacked sections as well as in the associated coherence sections (Figure 5c and d). The coherence values are close to one for CO samples located on the actual reflection event of the respective wave type and very low for all other samples.

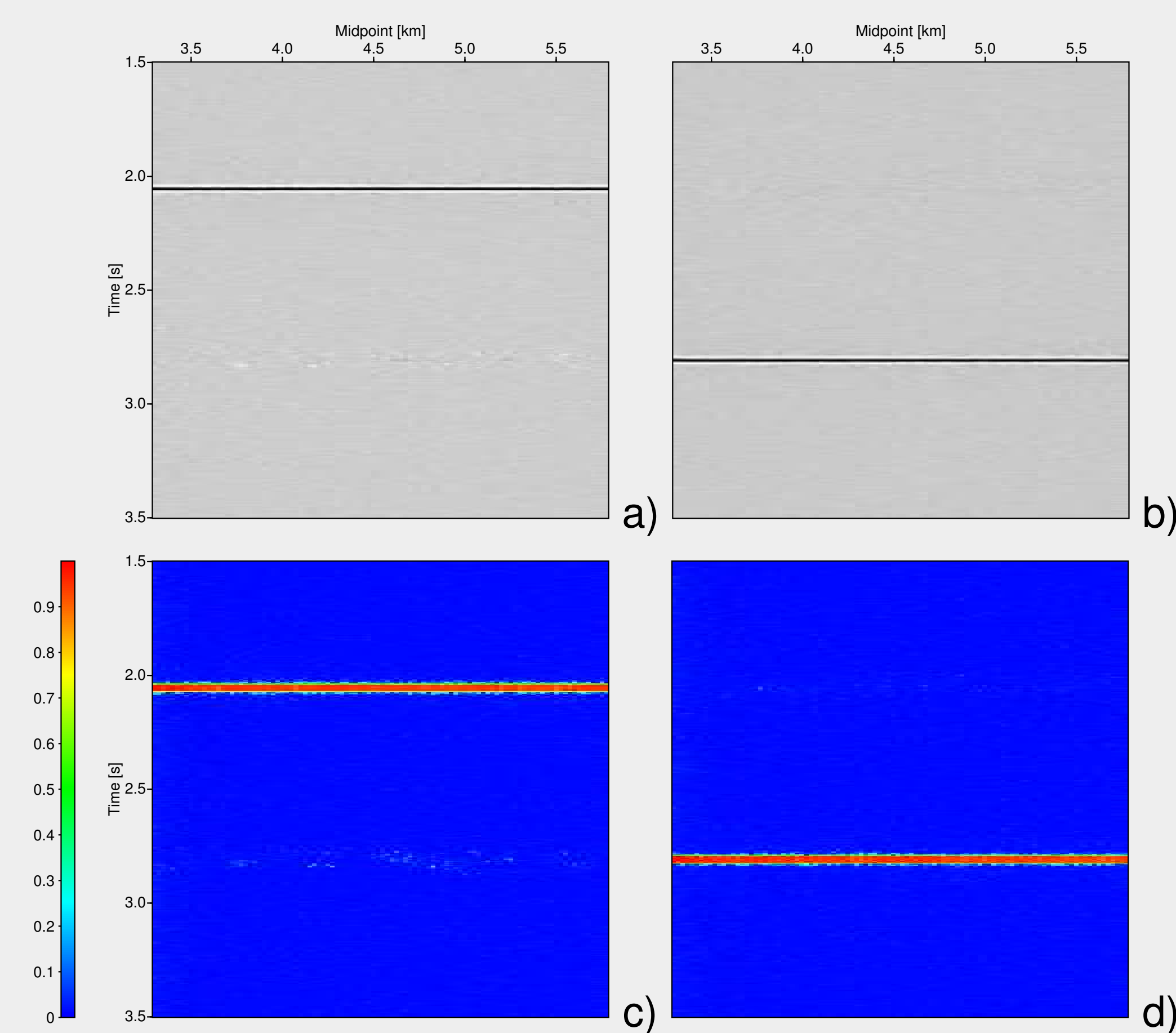


Figure 5: Upper part: a) PP and b) PS CO CRS stack section. Lower part: associated coherence sections for c) PP- and d) PS-reflections.

As the P-wave velocity at the sources as well as the P- and S-wave velocities at the receivers are known the kinematic wavefield attributes β_G , β_S , K_1 , K_2 , and K_3 can be computed. As an example, Figure 6 shows the incidence and emergence angles. The upper part depicts the obtained β_G -sections, the lower part the β_S -sections. The attributes for the PP-reflections are presented on the left hand side and for the PS-reflections on the right hand side. The wavefield attributes are reliable only for samples with sufficiently high coherence values.

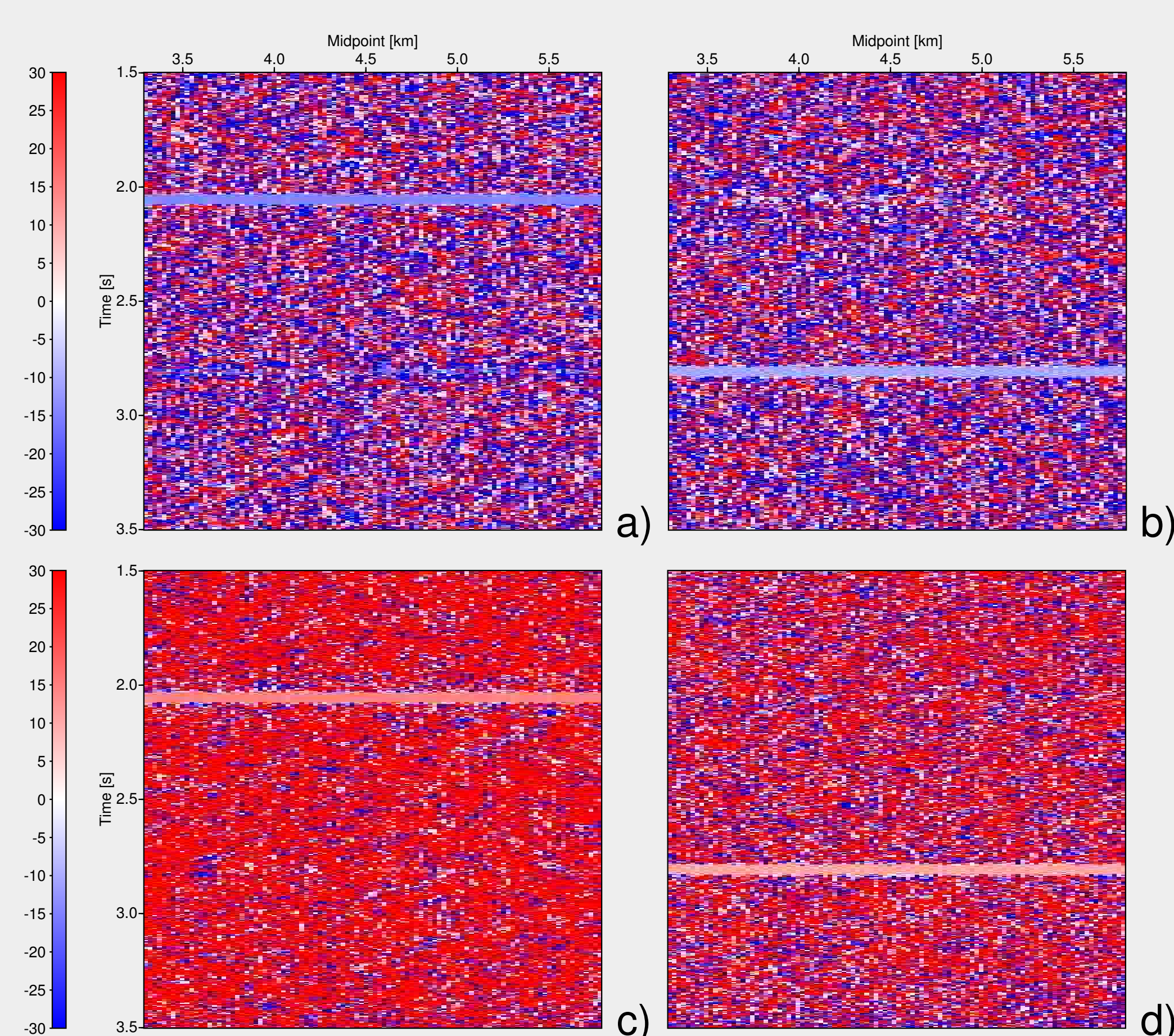


Figure 6: Kinematic wavefield attributes determined by the CO CRS stack. Upper part: β_G -sections [°] for a) PP- and b) PS-reflections. Lower part: β_S -sections [°] for c) PP- and d) PS-reflections.

Note that one observes slight residues of the PS-reflections in the PP stacked section as well as in the corresponding attribute and coherence sections, whereas there are almost no residues of the PP-event in the PS sections. This effect is caused by a modeling deficiency. While the P-wave polarization direction coincides exactly with the ray propagation direction, the polarization direction of the S-waves turned out to be not perfectly normal to the modeled rays and, thus, leaks through into the PP-sections.

Conclusions & Outlook

We have presented a new approach to handle multi-component data in the framework of the 2D CO CRS stack. This approach is able to distinguish between PP- and PS-reflections by combining operator shape and orientation with polarization information. It provides stacked sections and kinematic wavefield attribute sections separately for both wave types. An application to a simple synthetic land data set demonstrated that the approach is able to detect, clearly separate, and locally parameterize PP- and PS-events during the stack. Note that OBS data can be readily processed with the same strategy in case of a virtually horizontal seafloor.

The proposed approach can also be applied to other multi-component acquisition geometries like land seismics and OBS with varying surface/seafloor elevations as well as vertical seismic profiling (VSP). In these cases, different CRS stacking operators are required to approximate the reflection traveltimes, but the handling of polarization information remains the same. To investigate the actual potential of the approach presented here, tests with more realistic models as well as with real data are required. In the latter case, appropriate corrections are necessary to take the effect of the free surface (land data) or the effect of the seafloor (OBS data) into account. The introduced strategy to process multi-component data can also be transferred to the more general 3D case in order to handle three-component data.

References

- Bergler, S. (2001). The Common-Reflection-Surface Stack for Common Offset - Theory and Application. Master's thesis, University of Karlsruhe.
- Boelsen, T. (2005). The Common-Reflection-Surface Stack for arbitrary acquisition geometries and multi-component data - Theory and Application. Master's thesis, University of Karlsruhe.
- Boelsen, T. and Mann, J. (2005). 2D CO CRS stack for OBS and VSP data and arbitrary top-surface topography. In *Extended abstracts, 67th Conf. Eur. Assn. Geosci. Eng. Session P181*.
- Duveneck, E. (2004). Velocity model estimation with data-derived wavefront attributes. *Geophysics*, 69(1):265–274.
- Höcht, G., de Bazelaire, E., Majer, P., and Hubral, P. (1999). Seismics and optics: hyperbolae and curvatures. *J. Appl. Geophys.*, 42(3,4):261–281.
- Jäger, R., Mann, J., Höcht, G., and Hubral, P. (2001). Common-Reflection-Surface stack: image and attributes. *Geophysics*, 66(1):97–109.
- Mann, J., Jäger, R., Müller, T., Höcht, G., and Hubral, P. (1999). Common-Reflection-Surface stack - a real data example. *J. Appl. Geophys.*, 42(3,4):301–318.
- Müller, N.-A. (2005). 3-D inversion with kinematic wavefield attributes. In *Extended abstracts, 67th Conf. Eur. Assn. Geosci. Eng. Session B040*.
- Zhang, Y., Bergler, S., and Hubral, P. (2001). Common-Reflection-Surface (CRS) stack for common-offset. *Geophys. Prosp.*, 49(6):709–718.

Acknowledgments

This work was kindly supported by the sponsors of the *Wave Inversion Technology (WIT) Consortium*, Karlsruhe, Germany.

Related presentations

- B040** 3-D inversion with kinematic wavefield attributes, *N.-A. Müller*
- F042** Minimum-aperture Kirchhoff migration by means of CRS attributes, *C. Jäger*
- P012** CRS-stack-based seismic imaging considering top-surface topography, *von Steht et al.*
- P181** 2D CO CRS stack for OBS and VSP data and arbitrary top-surface topography, *Boelsen and Mann*
- W6-03** CRS-stack-based seismic imaging considering top-surface topography, *Z. Heilmann*
- W6-04** CRS-stack-based residual static correction - a real data example, *I. Koglin*
- W6-05** The application of CRS methods to a line from Saudi Arabia, *G. Gierse*